



**HAL**  
open science

# High-speed large-scale automated isolation of SARS-CoV-2 from clinical samples using miniaturized co-culture coupled to high-content screening

Rania Francis, Marion Le Bideau, Priscilla Jardot, Clio Grimaldier, Didier Raoult, Jacques Yaacoub Bou Khalil, Bernard La Scola

## ► To cite this version:

Rania Francis, Marion Le Bideau, Priscilla Jardot, Clio Grimaldier, Didier Raoult, et al.. High-speed large-scale automated isolation of SARS-CoV-2 from clinical samples using miniaturized co-culture coupled to high-content screening. *Clinical Microbiology and Infection*, 2021, 27 (1), pp.128.e1-128.e7. 10.1016/j.cmi.2020.09.018 . hal-03216089

**HAL Id: hal-03216089**

**<https://amu.hal.science/hal-03216089>**

Submitted on 2 Jan 2023

**HAL** is a multi-disciplinary open access archive for the deposit and dissemination of scientific research documents, whether they are published or not. The documents may come from teaching and research institutions in France or abroad, or from public or private research centers.

L'archive ouverte pluridisciplinaire **HAL**, est destinée au dépôt et à la diffusion de documents scientifiques de niveau recherche, publiés ou non, émanant des établissements d'enseignement et de recherche français ou étrangers, des laboratoires publics ou privés.



Distributed under a Creative Commons Attribution - NonCommercial 4.0 International License

**Original article**

**High-speed large-scale automated isolation of SARS-CoV-2 from  
clinical samples using miniaturized co-culture coupled to high-content  
screening**

1

2 **Rania Francis<sup>1,2</sup>, Marion Le Bideau<sup>2</sup>, Priscilla Jardot<sup>2</sup>, Clio Grimaldier<sup>2</sup>, Didier Raoult<sup>1,2</sup>,**

3 **Jacques Yaacoub Bou Khalil<sup>1\*</sup> and Bernard La Scola<sup>1,2\*</sup>**

4 <sup>1</sup>Institut Hospitalo-Universitaire Méditerranée-Infection, 19-21 Boulevard Jean Moulin, 13005,  
5 Marseille, France.

6 <sup>2</sup>Aix-Marseille Université, Institut de Recherche pour le Développement (IRD), UMR Microbes  
7 Evolution Phylogeny and Infections (MEPHI), AP-HM, 19-21 Boulevard Jean Moulin, 13005,  
8 Marseille, France.

9

10 Corresponding Authors: Bernard La Scola and Jacques Yaacoub Bou Khalil

11 **Mailing address:** Aix Marseille Univ, IRD, APHM, MEPHI, IHU-Méditerranée Infection

12 19-21 boulevard Jean Moulin, 13005 Marseille, France

13 Tel: +33-4-13-73-24-01

14 [bernard.la-scola@univ-amu.fr](mailto:bernard.la-scola@univ-amu.fr), [boukhaliljacques@gmail.com](mailto:boukhaliljacques@gmail.com)

15

16

17 **Abstract**

18 **Objectives:** A novel coronavirus, SARS-CoV-2, is responsible for the current COVID-19 global  
19 pandemic. Only a few laboratories routinely isolate the virus, which is because the current co-culture  
20 strategy is highly time-consuming and requires working in a biosafety level 3 laboratory. This work  
21 aimed to develop a new high-throughput isolation strategy using novel technologies for rapid and  
22 automated isolation of SARS-CoV-2.

23 **Methods:** We used an automated microscope based on high-content screening (HCS), and we  
24 applied specific image analysis algorithms targeting cytopathic effects of SARS-CoV-2 on Vero E6  
25 cells. A randomized panel of 104 samples, including 72 that tested positive by RT-PCR and 32 that  
26 tested negative, were processed with our HCS strategy and were compared to the classical isolation  
27 procedure.

28 **Results:** The isolation rate was 43% (31/72) with both strategies on RT-PCR-positive samples and  
29 was correlated with the initial RNA viral load in the samples, in which we obtained a positivity  
30 threshold of 27 Ct. Co-culture delays were shorter with the HCS strategy, where 80% (25/31) of the  
31 positive samples were recovered by the third day of co-culture, compared to only 26% (8/30) with the  
32 classic strategy. Moreover, only the HCS strategy allowed us to recover all the positive samples (31  
33 with HCS versus 27 with classic strategy) after 1 week of co-culture.

34 **Conclusions:** This system allows the rapid and automated screening of clinical samples with  
35 minimal operator workload, which reduces the risk of contamination, thus paving the way for future  
36 applications in clinical microbiology, such as large-scale drug susceptibility testing.

37 **Keywords:** COVID-19, SARS-CoV-2, co-culture, isolation, high-content screening.

38

## 39 **Introduction**

40 An outbreak caused by a novel coronavirus (SARS-CoV-2) occurred in late December 2019 in  
41 Wuhan, China; it then spread worldwide and was declared a pandemic by the WHO on the 12<sup>th</sup> of  
42 March 2020 [1],[2],[3]. Laboratory diagnosis is mainly based on molecular biology using specific  
43 RT-PCR systems to detect the virus in clinical samples [4],[5],[6]. However, during such pandemics,  
44 strain isolation is important, as having the particle represents the key to all in vitro research, such as  
45 drug susceptibility testing and vaccine development [7]. Furthermore, culture allows access to all  
46 viral genomes since whole-genome sequencing techniques performed directly on samples have their  
47 limitations in terms of sensitivity  
48 . A first application of this strategy was used by our group to evaluate the risk of contagiousness of  
49 patients for discharge from the infectious diseases ward [8]. However, the current co-culture strategy  
50 is tedious and time consuming, especially due to the large number of samples to be cultured. An ideal  
51 solution would be an automated system allowing the rapid screening and monitoring of co-cultures at  
52 large scale.

53 In previous works, we developed a screening strategy based on high-content screening microscopy  
54 (HCS) for the isolation of environmental giant viruses in amoeba and the strict intracellular  
55 bacterium *Coxiella burnetii* [9],[10]. In this work, we used the same automated high-throughput  
56 method and adapted it for SARS-CoV-2 isolation from clinical samples with the objective to discard  
57 the negative co-cultures after one week and omit blind subcultures. Specific algorithms were applied  
58 to detect cytopathic effects in co-cultures at high throughput, which eliminates the subjectivity  
59 related to manual observations by the laboratory personnel. This strategy exhibited a similar isolation  
60 rate but a lower co-culture delay when compared to the classic technique routinely used for isolation,  
61 as we were able to detect all positive co-cultures in one week.

## 62 **Methods**

### 63 **1. Co-culture process for the developmental stage**

64 For protocol development, we used Vero E6 cells (ATCC CRL-1586) as cellular support and the  
65 locally isolated SARS-CoV-2 strain IHUMI-3. This viral strain was previously isolated in our lab  
66 from a nasopharyngeal swab, as previously described [11]. The viral titer was calculated by the  
67 TCID50 method. Briefly, we cultured Vero E6 cells in black 96-well microplates with optical  
68 bottoms (Nunc, Thermo Fischer) at a concentration of  $2 \times 10^5$  cells/ml and a volume of 200  $\mu$ l per  
69 well in transparent MEM supplemented with 4% fetal calf serum and 1% glutamine. Plates were  
70 incubated for 24 hours at 37°C in a 5% CO<sub>2</sub> atmosphere to allow cell adhesion. Infection was then  
71 carried out with 50  $\mu$ l of the viral stock suspension diluted up to  $10^{-10}$ . The plates were centrifuged  
72 for 1 hour at 700xg, and the total volume per well was adjusted to 250  $\mu$ l with culture medium.  
73 Uninfected cells were considered negative controls.

## 74 **2. Detection process optimization**

75 DNA staining was performed with NucBlue™ Live ReadyProbes™ reagent (Molecular Probes, Life  
76 Technologies, USA). A concentration of 4 ng/ml was used (equivalent to 10  $\mu$ l per well directly from  
77 stock solution), and a different well was stained each day to avoid photobleaching and possible  
78 cytotoxicity, as previously described [10].

79 Image acquisition and analysis were performed using the automated CellInsight™ CX7 High-  
80 Content Analysis Platform coupled with an automation system including an Orbitor™ RS Microplate  
81 mover and an incubator Cytomat™ 2C-LIN (Thermo Scientific). The HCS Studio 3.1 software was  
82 used to set up acquisition parameters using a 20x objective (0.45 NA) and to define image analysis.  
83 Autofocus was performed on the fluorescence channel of the fluorescent probe NucBlue (386 nm).  
84 This channel served as a primary mask for cell detection and identification. The regions of interest  
85 (ROIs) were then identified on brightfield images as a Voronoi diagram derived from nuclear masks.  
86 Cell debris were removed using area cutoffs. The entire well (80 fields per well) was screened on a  
87 daily basis, and data were extracted and analyzed in a dedicated application that we recently

88 developed in R Studio® for the detection of the intracellular bacteria, *Coxiella burnetii* [10]. We  
89 optimized this application for the detection of cytopathic effects caused by COVID-19.  
90 Briefly, a database consisting of negative (uninfected cells) and positive (infected cells) controls was  
91 generated. The data were used to define specific features allowing the discrimination between the two  
92 groups. The following features were selected: the average, total and variation of the nuclear  
93 fluorescence intensity per cell, the nuclear area, the skewness of the brightfield intensity distribution,  
94 the kurtosis of the brightfield intensity distribution and the total intensity of the brightfield within the  
95 regions of interest (ObjectAvgIntenCh1, ObjectTotalIntenCh1, ObjectVarIntenCh1, ObjectAreaCh1,  
96 ROI\_SkewIntenCh3, ROI\_KurtIntenCh3 and ROI\_TotalIntenCh3 respectively). These parameters  
97 were used to generate two clusters using the K-means clustering algorithm, and the percentage of  
98 injured cells per well was calculated as previously described [10]. We then compared the percentage  
99 of injured cells obtained to the total cell count in each well to detect cell lysis.

$$\text{ratio} = \frac{\% \text{ injured cells}}{\text{Total cell count}}$$

### 101 **3. Large-scale co-culture of clinical samples**

102 We applied this strategy for the detection of SARS-CoV-2 in 104 randomly chosen, anonymized  
103 nasopharyngeal swab samples. Initial RT-PCR ranged from 12 Ct to 34 Ct in 72 samples, and 32  
104 samples with negative initial PCR were used as negative controls. All samples except five were from  
105 hospitalized patients. Sample preparation and co-culture were performed as previously described  
106 [11]. Briefly, 500 µl of the sample was processed into a 0.22-µm centrifugal filter (Merck millipore,  
107 Darmstadt, Germany) and was centrifuged at 12000xg for 5 minutes. Fifty microliters was then  
108 inoculated on a monolayer of Vero E6 cells cultured in 96-well microplates. A negative control  
109 consisting of uninfected cells and a positive control consisting of cells infected with a 10<sup>-4</sup> dilution of  
110 the IHUMI-3 strain were considered. A centrifugation step (700xg for 1 h) was performed to enhance  
111 the entrance of the virus into the cells. Plates were then incubated at 37°C and monitored for 7 days

112 to search for cytopathic effects. In parallel, the same samples were processed using the classical  
113 isolation strategy based on the manual observation of cytopathic effects under an inverted microscope  
114 to validate our strategy [11],[8],[12]. For this strategy, co-cultures showing no cytopathic effects after  
115 one week were sub-cultured at days 7 and 14 onto a fresh monolayer of cells for a complete  
116 observation of three weeks.

#### 117 **4. Results validation by scanning electron microscopy and RT-PCR**

118 Positive co-cultures were processed with both scanning electron microscopy (SEM) and RT-PCR  
119 directly from culture supernatant to validate the presence of COVID-19 viral particles. Briefly, SEM  
120 was performed using the SU5000 microscope (Hitachi High-Tech Corporation, Tokyo, Japan)  
121 allowing a rapid observation in approximately 10 minutes without time-consuming sample  
122 preparations [12]. The RT-PCR protocol was performed as previously described by Amrane et al.,  
123 targeting the E gene [13]. This RT-PCR was applied to wells showing a cytopathic effect to confirm  
124 that this effect was due to SARS-CoV-2 and to negative wells to confirm that the lack of cytopathic  
125 effect was not due to microscopically undetectable minimal viral growth.

#### 126 **5. Statistical analysis**

127 The R Studio® and XLSTAT software programs were used to perform all statistical tests included in  
128 this paper. P values were calculated to search for significant differences between the positivity rates  
129 obtained on a daily basis of co-culture using the HCS and the classic isolation strategies. ROC curves  
130 were also calculated to determine a positivity threshold for strain isolation related to the initial viral  
131 load in the samples (initial RT-PCR results on the samples) for the two strategies. These evaluations  
132 were performed on all 104 nasopharyngeal swab samples tested in this work.

#### 133 **6. Ethical statement**

134 According to the procedures of the French Commission for Data Protection (Commission Nationale  
135 de l'Informatique et des Libertés), collected data were anonymized. The study was approved by the

136 local ethics committee of IHU (Institut Hospitalo-Universitaire) - Méditerranée Infection (No. 2020-  
137 01).

## 138 **Results**

### 139 **1. Cytopathic effects and cell lysis detection**

140 Figure 1 presents the fluorescence and brightfield images acquired with the CX7 microscope at days  
141 1 and 6 post infection, showing the early stages of infection of SARS-CoV-2 (Supplementary Fig. 1 -  
142 a, b) compared to advanced stages of infection and cell lysis (Supplementary Fig. 1 - g, h, i, j, k).  
143 Typical cytopathic effects consist of an increasing nuclear fluorescence intensity of the NucBlue  
144 fluorescent probe, in addition to nuclear fragmentation. These observations resulted in increases in  
145 the average, total and variation intensity of the nucleus and a decrease in the nuclear area on the  
146 fluorescence images. Additionally, infected cells become round and form aggregates, resulting in  
147 increases in total intensity, skewness and kurtosis on the brightfield images. Finally, advanced stages  
148 of infection are represented by cell lysis.

### 149 **2. Automated detection results**

150 The data extracted from the images were analyzed in the dedicated application in R Studio. The  
151 database of negative and positive controls served as training data for the clustering algorithm, and a  
152 baseline of 2 to 3% injured cells was predicted in the negative training data compared to a value of 50  
153 to 55% injured cells in the positive training data. The percentage of injured cells in each condition  
154 was predicted and then divided by the total cell count per well. This ratio allowed us to distinguish  
155 positive wells, showing cytopathic effects or cell lysis, from the negative control wells consisting of  
156 uninfected cells (Figure 1- a). Cytopathic effects were detectable up until the dilution  $10^{-4}$  after 6  
157 days of culture for the strain IHUMI-3 used in this study, which corresponds to the viral titer  
158 obtained by TCID<sub>50</sub>.

159 Furthermore, the automation system allowed us to monitor co-culture on a daily basis without any  
160 intervention from the operators. The Momentum software was used to monitor the automation system

161 linked to the HCS microscope. A screening process was predefined, thus allowing the proper  
162 incubation of the plates followed by the automated handling of the screening process at each  
163 specified time point.

### 164 **3. Screening of clinical samples with the new HCS and the classic isolation strategies**

165 Among the panel of 104 samples processed on the CX7 microscope, 32 samples had a negative initial  
166 PCR and were considered controls for the system's sensitivity; therefore, the corresponding co-  
167 cultures were negative. Among the remaining 72 samples, we managed to isolate the virus from 31  
168 samples using our automated detection system. The detection delay ranged from 24 hours to 3 days  
169 for most samples and was prolonged to 6 days for samples with low viral load. Figure 1-b shows  
170 examples of co-culture results obtained with the automated detection system compared to the  
171 negative (uninfected cells) and positive (cells infected with the viral strain IHUMI-3) controls.  
172 Regarding the classic isolation strategy, 30 viral strains were isolated from the tested panel of  
173 samples, and the 32 samples with negative initial PCR had negative culture results as well. The  
174 majority of strains were recovered after four days of co-culture, and only a few were isolated at  
175 earlier stages. Three strains out of 30 were recovered after subcultures, two in the second week and  
176 one in the third week of co-culture.

177 A significantly higher percentage of positive samples was observed on a daily basis with the HCS  
178 strategy (Figure 2). Moreover, the majority of positive samples were isolated by the third day of co-  
179 culture using the HCS strategy, where 80% (25/31) positivity was obtained compared to only 26%  
180 (8/30) with the classic strategy (p value<0.001).

181 To validate our results, positive co-cultures were processed for scanning electron microscopy to  
182 confirm the presence of viral particles. We detected viral particles in the supernatants of all samples  
183 that were detected as positive by the HCS strategy. Figure 3 shows an example of particle detection  
184 in culture supernatant by SEM. RT-PCR performed on all wells correlated with the results of the  
185 microscopy-based detection.

186 Then, we correlated the isolation rates obtained with both strategies to the initial viral load (RT-PCR  
187 results) in each sample, and the results are shown in Figure 4. We obtained similar isolation rates  
188 with the HCS isolation strategy and with the classic strategy. Moreover, we observed that most of the  
189 strains were recovered from samples with an initial viral load lower than 30 Ct with both strategies,  
190 and in most cases, isolation failed from samples with higher Ct values. Therefore, we calculated the  
191 positivity threshold of the isolation rate compared to the initial viral load in the samples using an  
192 ROC curve, and we obtained a similar positivity threshold of 27 Ct for both isolation strategies  
193 (Figure 5).

## 194 **Discussion**

195 In this work, we were able to co-culture a large amount of clinical samples and monitor them with a  
196 fully automated system, which reduced the workload and time required from laboratory technicians.  
197 Similar isolation rates were obtained with both isolation strategies, which validated the efficiency of  
198 our new automated system. Moreover, this isolation rate was obtained in one week with the HCS  
199 strategy without any further subcultures, contrary to the classic technique with weekly subcultures for  
200 a total incubation time of three weeks. The main advantage of this technique relies in the automation,  
201 as it limits the risks of exposure or contamination of the personnel, since plate monitoring and data  
202 analysis can be carried out from a distance, thus avoiding direct contact and manual observations of  
203 co-cultures. Furthermore, since the loss of virus cultivability in samples allows us to consider the  
204 patients at low risk of contamination, it therefore helps in the decision making to discharge them  
205 from the infectious diseases wards [8]. The use of the HCS isolation strategy allowed us to answer  
206 this question in one week. This is especially critical at the beginning of an epidemic or when PCR  
207 detection systems have to be modified. Moreover, several studies showed that assessing the duration  
208 of SARS-CoV-2 infectivity is based on viral cell culture or secondary infection rates  
209 [12],[14],[15],[16],[17],[18],[19]. Therefore, our automated isolation system allows answering this  
210 question faster than any other tool, and viral infectivity can be assessed several times during the

211 outbreak to search for modifications, such as reduced transmissibility or effect of antiviral therapy.  
212 Furthermore, the greater the number of strains isolated, the better the understanding of the genetic  
213 diversity of this virus, especially since genome sequencing directly from samples is limited to the  
214 viral load, and a very poor genome assembly is obtained when the viral load is greater than 19 Ct  
215 [20],[19]. Subsequently, developing an automated viral isolation technique was necessary to  
216 overcome the subjective and time-consuming manual microscopic observations. This new strategy is  
217 therefore applicable during the current crisis to recover strains from suspected samples in a safe and  
218 rapid way. Further work is underway to apply this technique for the large-scale drug susceptibility  
219 testing of SARS-CoV-2 strains isolated from patients. Finally, the algorithms used here could be  
220 adapted and applied for the detection and isolation of other viruses from clinical samples in cases of  
221 known and emerging viral diseases.

#### 222 **Transparency declaration**

223 Authors would like to declare that Didier Raoult is a consultant for Hitachi High-Tech Corporation.

#### 224 **Author Contributions**

225 JYBK and BLS conceived the project. RF and JYBK developed the HCS methodology. RF, MLB, PJ  
226 and CG conducted the experiments. RF and JYBK conducted the analysis. RF, DR, JYBK and BLS  
227 wrote the manuscript.

#### 228 **Funding**

229 This work was supported by a grant from the French State managed by the National Research  
230 Agency under the "Investissements d'avenir (Investments for the Future)" program under the  
231 reference ANR-10-IAHU-03 (Méditerranée Infection) and by the Région Provence-Alpes-Côte-  
232 d'Azur and the European funding FEDER PRIM1.

#### 233 **Acknowledgments**

234 We sincerely thank Takashi Irie, Kyoko Imai, Shigeki Matsubara, Taku Sakazume, Toshihide  
235 Agemura, Yusuke Ominami, Hisada Akiko and the Hitachi team in Japan Hitachi High-Tech

236 Corporation (Toranomon Hills Business Tower, 1-17-1 Toranomon, Minato-ku, Tokyo 105-6409,  
237 Japan) for the collaborative study conducted together with IHU Méditerranée Infection, and for the  
238 installation of a SU5000 microscope at the IHU Méditerranée Infection facility.

## 239 **References**

- 240 [1] WHO Director-General's opening remarks at the Mission briefing on COVID-19 - 12 March  
241 2020 n.d. [https://www.who.int/dg/speeches/detail/who-director-general-s-opening-remarks-at-](https://www.who.int/dg/speeches/detail/who-director-general-s-opening-remarks-at-the-mission-briefing-on-covid-19---12-march-2020)  
242 [the-mission-briefing-on-covid-19---12-march-2020](https://www.who.int/dg/speeches/detail/who-director-general-s-opening-remarks-at-the-mission-briefing-on-covid-19---12-march-2020) (accessed April 2, 2020).
- 243 [2] Lai CC, Shih TP, Ko WC, Tang HJ, Hsueh PR. Severe acute respiratory syndrome coronavirus  
244 2 (SARS-CoV-2) and coronavirus disease-2019 (COVID-19): The epidemic and the  
245 challenges. *Int J Antimicrob Agents* 2020;55:105924. doi:10.1016/j.ijantimicag.2020.105924.
- 246 [3] Zhu N, Zhang D, Wang W, Li X, Yang B, Song J, et al. A novel coronavirus from patients  
247 with pneumonia in China, 2019. *N Engl J Med* 2020;382:727–33.  
248 doi:10.1056/NEJMoa2001017.
- 249 [4] Tang Y-W, Schmitz JE, Persing DH, Stratton CW. The Laboratory Diagnosis of COVID-19  
250 Infection: Current Issues and Challenges. *J Clin Microbiol* 2020. doi:10.1128/JCM.00512-20.
- 251 [5] Chu DKW, Pan Y, Cheng SMS, Hui KPY, Krishnan P, Liu Y, et al. Molecular Diagnosis of a  
252 Novel Coronavirus (2019-nCoV) Causing an Outbreak of Pneumonia. *Clin Chem*  
253 2020;66:549–55. doi:10.1093/clinchem/hvaa029.
- 254 [6] Chan JF-W, Yip CC-Y, To KK-W, Tang TH-C, Wong SC-Y, Leung K-H, et al. Improved  
255 molecular diagnosis of COVID-19 by the novel, highly sensitive and specific COVID-19-  
256 RdRp/HeI real-time reverse transcription-polymerase chain reaction assay validated in vitro  
257 and with clinical specimens . *J Clin Microbiol* 2020. doi:10.1128/jcm.00310-20.
- 258 [7] Wang L-S, Wang Y-R, Ye D-W, Liu Q-Q. A review of the 2019 Novel Coronavirus (COVID-  
259 19) based on current evidence. *Int J Antimicrob Agents* 2020:105948.  
260 doi:10.1016/j.ijantimicag.2020.105948.

- 261 [8] La Scola B, Le Bideau M, Andreani J, Hoang VT, Grimaldier C, Colson P, et al. Viral RNA  
262 load as determined by cell culture as a management tool for discharge of SARS-CoV-2  
263 patients from infectious disease wards. *Eur J Clin Microbiol Infect Dis* Off Publ Eur Soc Clin  
264 Microbiol 2020;1. doi:10.1007/s10096-020-03913-9.
- 265 [9] Francis R, Ominami Y, Bou Khalil JY, La Scola B. High-throughput isolation of giant viruses  
266 using high-content screening. *Commun Biol* 2019. doi:10.1038/s42003-019-0475-6.
- 267 [10] Francis R, Mioulane M, Le Bideau M, Mati M-C, Fournier P-E, Raoult D, et al. High-Content  
268 Screening, a Reliable System for *Coxiella burnetii* Isolation from Clinical Samples . *J Clin*  
269 *Microbiol* 2020;58. doi:10.1128/jcm.02081-19.
- 270 [11] Gautret P, Lagier J-C, Parola P, Hoang VT, Meddeb L, Mailhe M, et al. Hydroxychloroquine  
271 and azithromycin as a treatment of COVID-19: results of an open-label non-randomized  
272 clinical trial. *Int J Antimicrob Agents* 2020:105949. doi:10.1016/j.ijantimicag.2020.105949.
- 273 [12] Colson P, Lagier JC, Baudoin JP, Bou Khalil J, La Scola B, Raoult D. Ultrarapid diagnosis,  
274 microscope imaging, genome sequencing, and culture isolation of SARS-CoV-2. *Eur J Clin*  
275 *Microbiol Infect Dis* 2020;39:1601–3. doi:10.1007/s10096-020-03869-w.
- 276 [13] Amrane S, Tissot-Dupont H, Doudier B, Eldin C, Hocquart M, Mailhe M, et al. Rapid viral  
277 diagnosis and ambulatory management of suspected COVID-19 cases presenting at the  
278 infectious diseases referral hospital in Marseille, France, - January 31st to March 1st, 2020: A  
279 respiratory virus snapshot. *Travel Med Infect Dis* 2020:101632.  
280 doi:10.1016/j.tmaid.2020.101632.
- 281 [14] Wölfel R, Corman VM, Guggemos W, Seilmaier M, Zange S, Müller MA, et al. Virological  
282 assessment of hospitalized patients with COVID-2019. *Nature* 2020;581:465–9.  
283 doi:10.1038/s41586-020-2196-x.
- 284 [15] Young BE, Ong SWX, Ng LF, Anderson DE, Chia WN, Chia PY, et al. Immunological and  
285 Viral Correlates of COVID-19 Disease Severity: A Prospective Cohort Study of the First 100

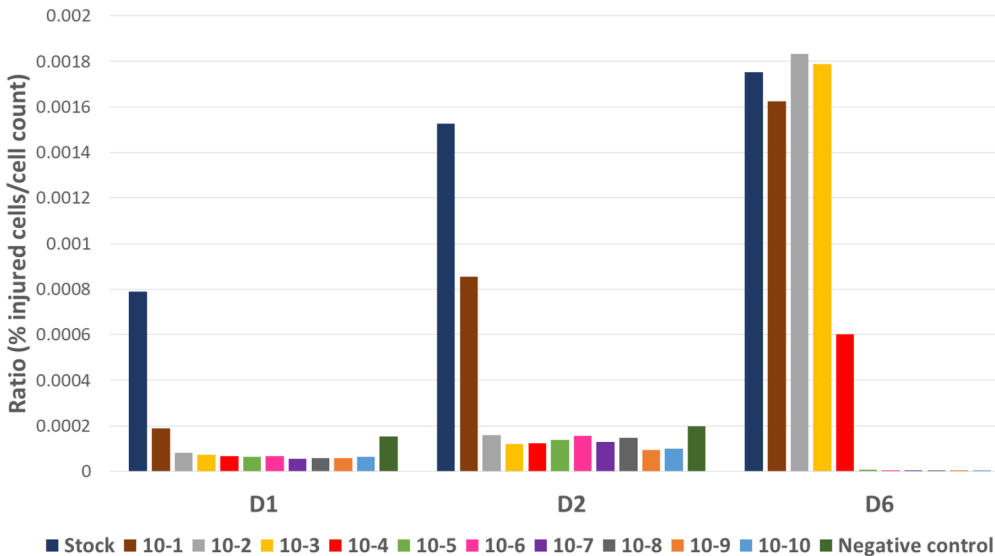
- 286 Patients in Singapore. SSRN Electron J 2020. doi:10.2139/ssrn.3576846.
- 287 [16] Million M, Lagier JC, Gautret P, Colson P, Fournier PE, Amrane S, et al. Early treatment of  
288 COVID-19 patients with hydroxychloroquine and azithromycin: A retrospective analysis of  
289 1061 cases in Marseille, France. *Travel Med Infect Dis* 2020;35.  
290 doi:10.1016/j.tmaid.2020.101738.
- 291 [17] Bullard J, Dust K, Funk D, Strong JE, Alexander D, Garnett L, et al. Predicting infectious  
292 SARS-CoV-2 from diagnostic samples. *Clin Infect Dis* 2020. doi:10.1093/cid/ciaa638.
- 293 [18] Kampen JJA van, Vijver DAMC van de, Fraaij PLA, Haagmans BL, Lamers MM, Okba N, et  
294 al. Shedding of infectious virus in hospitalized patients with coronavirus disease-2019  
295 (COVID-19): duration and key determinants. *MedRxiv* 2020;2019:2020.06.08.20125310.  
296 doi:10.1101/2020.06.08.20125310.
- 297 [19] Lu J, Peng J, Xiong Q, Liu Z, Lin H, Tan X, et al. Clinical immunological and virological  
298 characterization of COVID-19 patients that test re-positive for SARS-CoV-2 by RT-PCR.  
299 *Medrxiv* 2020:1–26. doi:10.1101/2020.06.15.20131748.
- 300 [20] Ahn D-G, Shin H-J, Kim M-H, Lee S, Kim H-S, Myoung J, et al. Current Status of  
301 Epidemiology, Diagnosis, Therapeutics, and Vaccines for Novel Coronavirus Disease 2019  
302 (COVID-19). *J Microbiol Biotechnol* 2020;30:313–24. doi:10.4014/jmb.2003.03011.

### 303 **Figure legends**

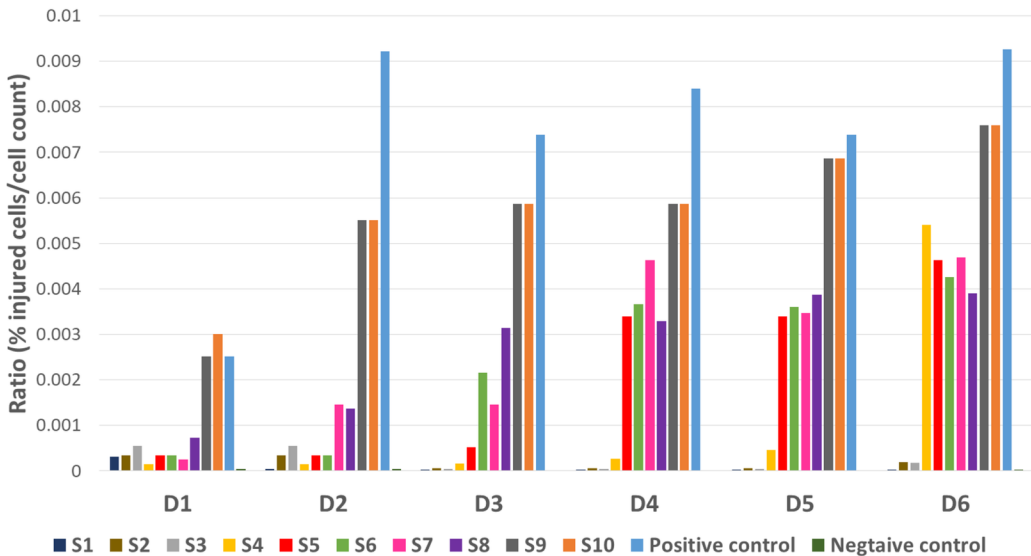
304 **Figure 1:** Automated detection of SARS-CoV-2 in co-culture. (a) Ratio of the percentage of injured  
305 cells on the total cell count of SARS-CoV-2-infected cells at different concentrations compared to the  
306 negative control over a period of 6 days. (b) Ratio of the percentage of injured cells on the total cell  
307 count of 10 clinical samples with different initial viral loads over a period of 6 days. Initial viral  
308 loads were negative in S1 and S2, 32 Ct in S3, 30 Ct in S4, 29 Ct in S5, 28 Ct in S6, 23 Ct in S7, 22  
309 Ct in S8, 16 Ct in S9 and 15 Ct in S10.

310 **Figure 2:** Cumulative percentage of isolated strains per day using the classic and the new HCS  
311 isolation strategies for samples detected as positive in co-culture. **Figure 3:** SEM images obtained  
312 with the SU5000 microscope showing SARS-CoV-2 particles isolated from clinical samples (white  
313 arrows). Acquisition settings and scale bars are generated on the original micrographs.  
314 **Figure 4:** Isolation rate of SARS-CoV-2 from nasopharyngeal samples according to initial Ct values  
315 in samples using the classic and the new HCS isolation strategies (40 Ct represents the samples with  
316 a negative initial PCR). Note that the curves are overlapping before 28 Ct, showing similar isolation  
317 rates for both strategies.  
318 **Figure 5:** Receiver operating characteristic (ROC) curves and positivity threshold analysis for  
319 positive samples detected by the classic (a) and the HCS (b) isolation strategies.

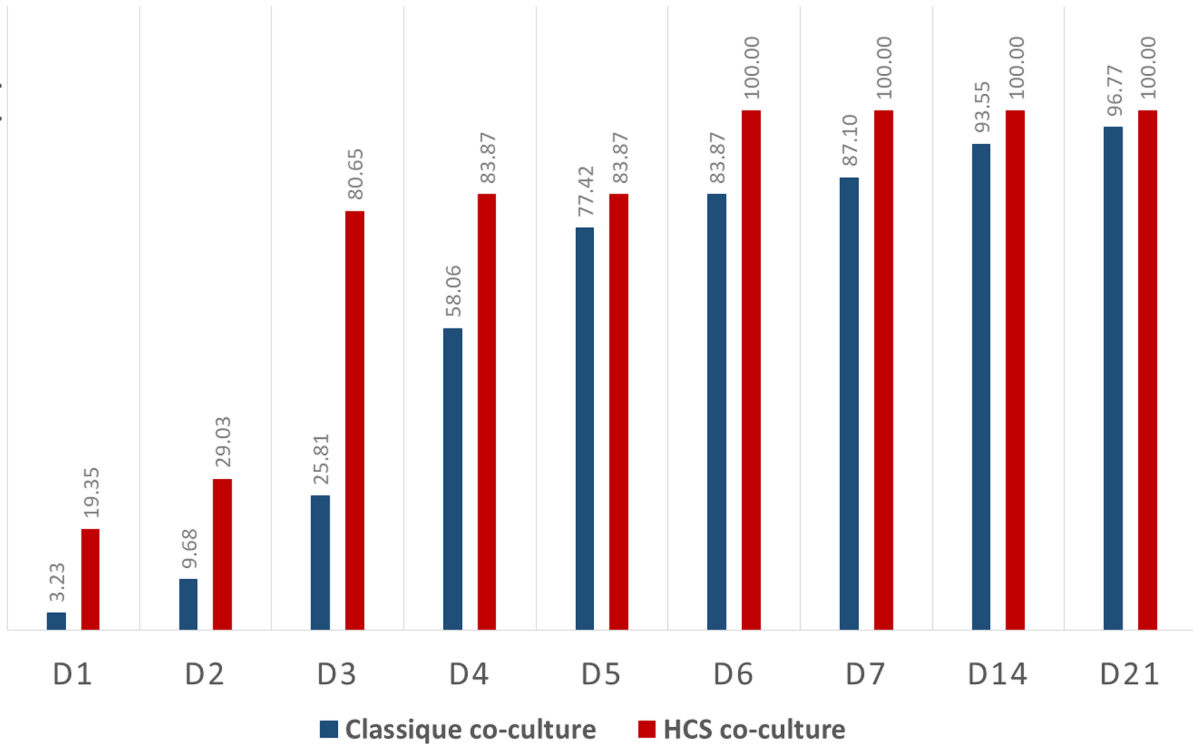
## a TCID50

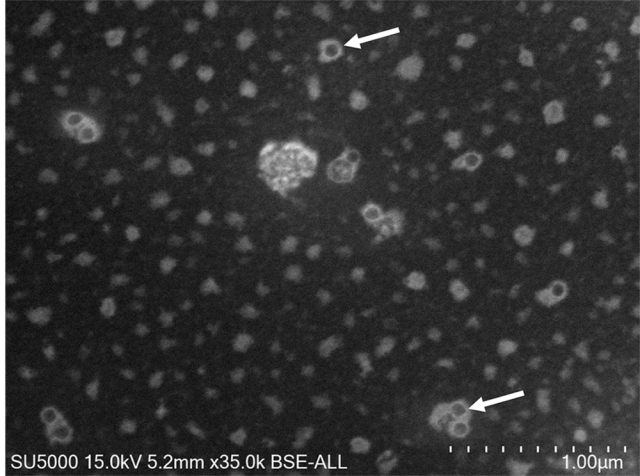
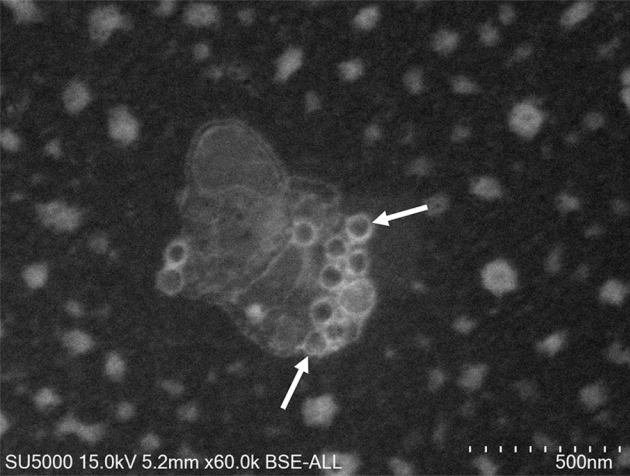


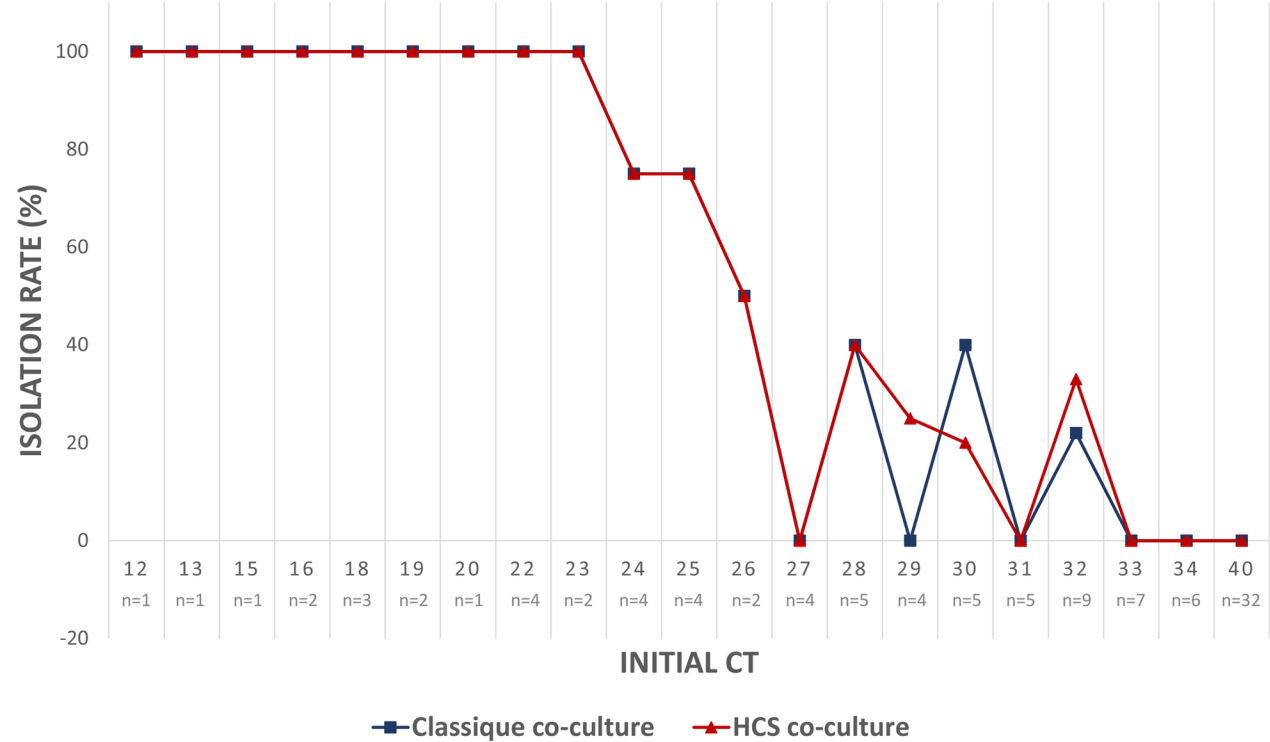
## b Clinical samples

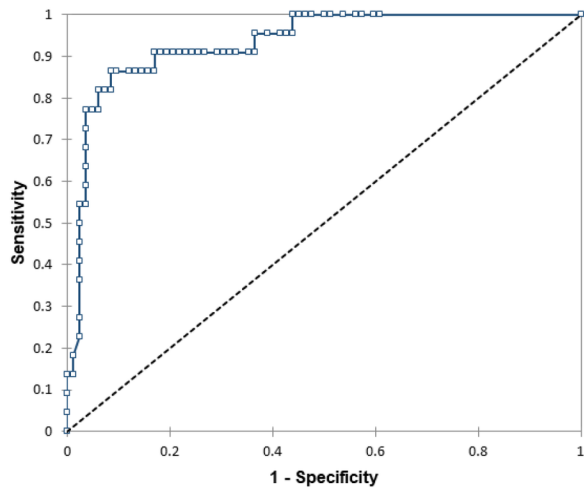


# CUMULATIVE ISOLATION RATE (%)

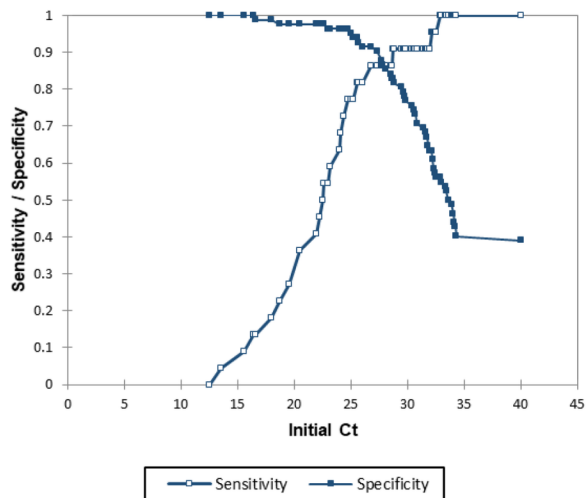
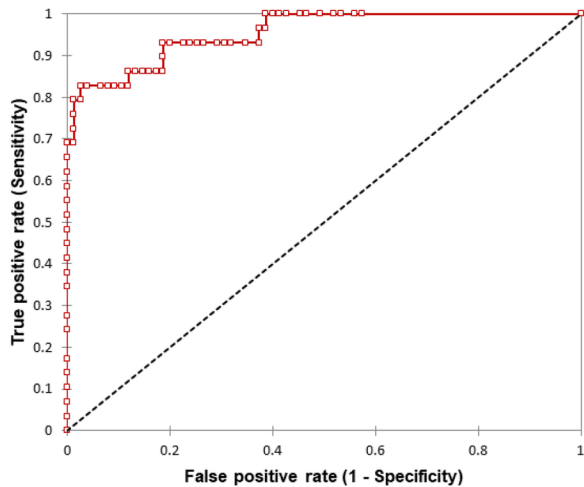






**a** ROC Curve / Initial Ct / AUC=0.932

Sensitivity and specificity / Initial Ct

**b** ROC Curve / Initial Ct / AUC=0.954

Sensitivity and specificity / Initial Ct

